

The high-temperature rotation-vibration spectrum and rotational clustering of silylene (SiH_2)

Victoria H. J. Clark, Alec Owens, Jonathan Tennyson, Sergei N. Yurchenko

*Department of Physics and Astronomy, University College London, Gower Street,
WC1E 6BT London, United Kingdom*

Abstract

A rotation-vibration line list for the electronic ground state (\tilde{X}^1A_1) of SiH_2 is presented. The line list, named CATS, is suitable for temperatures up to 2000 K and covers the wavenumber range 0–10 000 cm^{-1} (wavelengths $> 1.0 \mu\text{m}$) for states with rotational excitation up to $J = 52$. Over 310 million transitions between 593 804 energy levels have been computed variationally with a new empirically refined potential energy surface, determined by refining to 75 empirical term values with $J \leq 5$ and a newly computed high-level *ab initio* dipole moment surface. This is the first, comprehensive high-temperature line list to be reported for SiH_2 and it is expected to aid the study of silylene in plasma physics, industrial processes and possible astronomical detection. Furthermore, we investigate the phenomenon of rotational energy level clustering in the spectrum of SiH_2 . The CATS line list is available from the ExoMol database (www.exomol.com) and the CDS database.

Keywords: Molecular data, Line lists, Radiative transfer, Databases, ExoMol, Rotational clustering

1. Introduction

The spectrum of SiH_2 , known as silylene or silicon dihydride, was first observed in the late 1960s [1] and, since then, numerous experimental and theoretical studies have followed (see Ref. [2] and references within). Its

Email address: s.yurchenko@ucl.ac.uk (Sergei N. Yurchenko)
Preprint submitted to JQSRT

April 3, 2020

importance in silicon chemistry is largely owing to it being an intermediate in many chemical reactions involving silane (SiH_4). For example, the formation of SiH_2 is used to monitor the decomposition of SiH_4 into silylene and hydrogen; and the loss of SiH_2 can be used to track the formation of disilane (Si_2H_6) [3–5]. Given the widespread use of silane plasmas in industry, detailed spectroscopic information on SiH_2 can significantly help the detection and monitoring of certain processes, such as the deposition of hydrogenated amorphous silicon (a-Si:H) films, the chemistry of which is not fully understood [6]. Silylene is yet to be conclusively detected astronomically with unsuccessful searches in the circumstellar envelope of the carbon star IRC+10216 [7, 8], despite speculation of its presence in these environments [9].

Theoretical work on SiH_2 has primarily focused on *ab initio* predictions of the electronic state ordering relative to the isovalent methylene (CH_2), which interestingly has a triplet ground state (see Refs. [10, 11] and references within). More closely related to this study are the full-dimensional variational calculations of the ro-vibrational and ro-vibronic spectra of the ground and excited singlet states, \tilde{X}^1A_1 , \tilde{A}^1B_1 and \tilde{B}^1A_1 [12–14]. Nowadays, variational approaches are more robust and can offer high-accuracy predictions of line positions and intensities over extended wavenumber ranges, capable of supporting high-resolution spectroscopic measurements [15]. In particular, they have found widespread application in exoplanetary science through the ExoMol database [16, 17], which provides molecular line lists on a large variety of small molecules relevant to the atmospheric characterization of exoplanets and other hot bodies. In particular the ExoMol database already contains line lists for a number of silicon-bearing molecules: SiH_4 [18], SiH [19], SiO [20] and SiS [21]. It is within the ExoMol computational framework [22] that we treat silylene.

In this paper, we present a comprehensive molecular line list for the ground electronic state \tilde{X}^1A_1 of SiH_2 . The line list, named CATS, has been computed using robust first-principles methodologies with a degree of empirical tuning to the available spectroscopic data, namely the refinement of a newly computed high-level *ab initio* potential energy surface (PES) to experimentally determined ro-vibrational term values. The CATS line list is applicable for temperatures up to $T = 2000$ K and contains over 254 million transitions between states with rotational excitation up to $J = 51$.

Interestingly, triatomic symmetrical hydrides of the form XH_2 with a heavy central nuclei X and an interbond angle close to 90° exhibit well

separated, near-degenerate rotational energy level clusters at high rotational excitation [23]. This effect arises in local-mode molecules when the bonds are nearly orthogonal to each other such that the rotation of the molecule is not destabilized by Coriolis-type interactions with the vibrational modes. The new CATS line list is used to explore this phenomenon in SiH₂, which has an interbond angle $\alpha_e = 92.04^\circ$ [2] and is expected to form rotational cluster states at high rotational excitation.

The paper is structured as follows: In Sec. 2 we describe the theoretical approach including the construction of the PES and subsequent empirical refinement, the dipole moment surface (DMS) and the variational calculations used to produce the line list. In Sec. 3, the line list is presented and evaluated along with analysis of the temperature-dependent partition function. In Sec. 4, rotational energy level clustering in SiH₂ is investigated. Conclusions are offered in Sec. 5.

2. Theoretical approach

2.1. Potential Energy Surface

The initial *ab initio* PES was computed using the explicitly correlated coupled cluster method CCSD(T)-F12c [24] with the F12-optimized correlation consistent basis set, cc-pVQZ-F12 [25] in the frozen core approximation. Calculations employed the diagonal fixed amplitude ansatz 3C(FIX) [26] and a Slater geminal exponent value of $\beta = 1.0 a_0^{-1}$ [27]. The auxiliary basis sets were chosen to be the resolution of the identity OptRI [28] basis and the cc-pV5Z/JKFIT [29] and aug-cc-pwCV5Z/MP2FIT [30] basis sets for density fitting. MOLPRO2015 [31] was used for all electronic structure calculations. The PES was computed on a uniformly-spaced grid of 1898 nuclear geometries with energies up to $hc \cdot 19300 \text{ cm}^{-1}$ (h is the Planck constant and c is the speed of light). The grid was built in terms of three internal coordinates: the two Si-H bond lengths $1.2 \leq r_{\text{SiH}_1}, r_{\text{SiH}_2} \leq 2.0 \text{ \AA}$ and the interbond angle $30 \leq \alpha(\text{H}_1\text{SiH}_2) \leq 160^\circ$.

The three coordinates of the PES were chosen to be,

$$y_1 = 1 - \exp(-b(r_1 - r_e)), \quad (1)$$

$$y_2 = 1 - \exp(-b(r_2 - r_e)), \quad (2)$$

$$y_3 = \cos \alpha - \cos \alpha_e, \quad (3)$$

where r_1 and r_2 are the bond lengths Si-H₁ and Si-H₂, respectively, b is the Morse parameter, α is the interbond angle $\angle(\text{H-Si-H})$, and r_e and α_e are

the corresponding equilibrium parameters. The PES was represented using the analytical function [32],

$$V = V_0 + V_{\text{HH}}, \quad (4)$$

where

$$V_0 = \sum_{0 \leq i+j+k \leq 6} f_{ijk} y_1^i y_2^j y_3^k, \quad (5)$$

and

$$V_{\text{HH}} = B_1 \exp(-g_1 r_{\text{HH}}) + B_2 \exp(-g_2 r_{\text{HH}}^2). \quad (6)$$

The f_{ijk} expansion parameters obey the symmetric relation $f_{ijk} = f_{jik}$ owing to the identical properties of the hydrogen atoms 1 and 2. The distance between the hydrogen nuclei

$$r_{\text{HH}} = \sqrt{r_1^2 + r_2^2 - 2r_1 r_2 \cos \alpha}, \quad (7)$$

and the numerical parameters B_1 , B_2 , g_1 and g_2 are taken as in Ref. [32] (see supplementary material for values). The contribution V_{HH} is to prevent holes appearing in the PES at geometries where r_{HH} is small. The *ab initio* data was weighted with factors of the form [33]

$$w_i = \left(\frac{\tanh \left[-0.0008 \times (\tilde{E}_i - 12\,000) \right] + 1.002002002}{2.002002002} \right). \quad (8)$$

Watson's robust fitting scheme [34] was also utilized to reduce the weights of outliers and improve the description at lower energies. A total of 53 parameters were varied (46 expansion parameters + 2 equilibrium parameters + 1 Morse parameter + 4 damping parameters) in a least-squares fitting to the *ab initio* data which were reproduced with a weighted root-mean-square (rms) error of 0.0048 cm^{-1} .

2.2. Dipole Moment Surface

To represent the instantaneous dipole moment vector $\boldsymbol{\mu}$ of SiH_2 , we employed the so-called *pq* axis system [35]. The *p* and *q* axes were defined in the plane of the three nuclei with origin at the Si atom. The *q* axis bisects the interbond angle and the *p* axis lies perpendicular to the *q* axis. In electronic structure calculations, an external electric field with components ± 0.005 a.u. was applied along each axis and the respective dipole moment component

μ_p and μ_q determined using central finite differences. Calculations were at the same level of theory as the PES, namely CCSD(T)-F12c/cc-pVQZ-F12 and used the same grid of 1898 nuclear geometries.

In order to represent the two dipole components analytically the following expansions were used [36] (see also Ref. [37]),

$$\mu^{(q)} = \sin \alpha \sum_{i+j+k \leq 5} F_{ijk}^{(q)} \xi_1^i \xi_2^j \xi_3^k, \quad (9)$$

$$\mu^{(p)} = \sum_{i+j+k \leq 5} F_{ijk}^{(p)} \xi_1^i \xi_2^j \xi_3^k, \quad (10)$$

where the coordinates

$$\xi_1 = r_1 - r_e, \quad (11)$$

$$\xi_2 = r_2 - r_e, \quad (12)$$

$$\xi_3 = \cos \alpha - \cos \alpha_e. \quad (13)$$

The dipole expansion parameters $F_{ijk}^{(q)}$ and $F_{ijk}^{(p)}$ are subject to the conditions that the function $\mu^{(q)}$ is unchanged under the interchange of the identical protons, whereas the function $\mu^{(p)}$ is antisymmetric under this operation. The same analytic representation of the DMS was first used for CH₂ [35] and also previously for SiH₂ [13].

The dipole expansion parameters were determined through a least-squares fitting to the *ab initio* data. The same weight factors as given in Eq. (8) were used along with Watson’s robust fitting scheme and the equilibrium parameters fixed to $r_e = 1.514 \text{ \AA}$ and $\alpha_e = 92.0^\circ$. The μ_p component required 20 parameters (including the 2 equilibrium parameters) and reproduced the *ab initio* data with a weighted rms error of 1.5×10^{-4} D with the μ_q component using 26 parameters (including the 2 equilibrium parameters) giving a weighted rms error of 1×10^{-3} D. The DMSs of SiH₂ are provided in the supplementary material. Our *ab initio* dipole moment at the equilibrium (0.066 D) is in a good agreement with the *ab initio* equilibrium dipole moment reported by Gabriel *et al.* [12] (0.075 D) and slightly smaller than the equilibrium dipole moment from Ref. [13] (0.14 D).

2.3. Variational calculations

Variational calculations were performed with the nuclear motion program TROVE [38] and details of its methodology are discussed extensively elsewhere [22, 38–40]. Here, we summarise the main calculation steps.

The TROVE kinetic energy operator was constructed as a sixth-order Taylor expansion around the SiH₂ equilibrium geometry in terms of the following linearized coordinates,

$$\chi_1^{\text{lin}} = r_1^{\text{lin}} - r_e, \quad (14)$$

$$\chi_2^{\text{lin}} = r_2^{\text{lin}} - r_e, \quad (15)$$

$$\chi_3^{\text{lin}} = \alpha^{\text{lin}} - \alpha_e. \quad (16)$$

where r_i^{lin} and α^{lin} are the linearized versions of r_i and α , respectively (see Ref. [38]). The PES was also re-expanded to sixth-order in terms of the coordinates

$$\zeta_1^{\text{lin}} = 1 - \exp(-b(r_1^{\text{lin}} - r_e)), \quad (17)$$

$$\zeta_2^{\text{lin}} = 1 - \exp(-b(r_2^{\text{lin}} - r_e)), \quad (18)$$

$$\zeta_3^{\text{lin}} = \alpha^{\text{lin}} - \alpha_e. \quad (19)$$

For the primitive basis set, TROVE uses 1D numerical basis functions $\phi_{n_1}(\chi_1)$, $\phi_{n_2}(\chi_2)$ and $\phi_{n_3}(\chi_3)$ constructed with the Numerov-Cooley approach [41, 42]. The eigenfunctions of the 1D stretching and bending Hamiltonian operators $\hat{H}_i^{(1D)}$ were obtained by freezing all other degrees of freedom at their equilibrium values. In order to improve the primitive basis set by making it more compact, a two-step contraction scheme is used. At step 1, the 1D basis functions are combined into two subgroups, one for the stretches

$$\phi_{n_1, n_2}^{(2D)}(\chi_1, \chi_2) = \phi_{n_1}(\chi_1)\phi_{n_2}(\chi_2), \quad (20)$$

and the other for the bending mode,

$$\phi_{n_3}^{(1D)}(\chi_3) = \phi_{n_3}(\chi_3) \quad (21)$$

and these are used to solve the respective reduced Hamiltonian operators (stretching $\hat{H}^{(2D)}$ and bending $\hat{H}^{(1D)}$). The reduced Hamiltonians are constructed by averaging the total vibrational Hamiltonian operator $\hat{H}^{(J=0)}$ over the other ground vibrational basis functions [43, 44]. The resulting eigenfunctions of the two reduced problems, $\psi_{\lambda_1, \lambda_2}^{(2D)}$ and $\psi_{\lambda_3}^{(1D)}$, are contracted and classified according to the $\mathcal{C}_{2v}(\text{M})$ symmetry group [45] using an optimized symmetrization procedure [40] to form a symmetry-adapted 3D vibrational basis set as a product $\psi_{\lambda_1 \lambda_2}^{(2D)} \psi_{\lambda_3}^{(1D)}$. This vibrational basis set is then used for the $J = 0$ eigenproblem at step 2, with the eigenfunctions contracted again and used to form the symmetry-adapted $J > 0$ ro-vibrational basis set.

In steps 1 and 2 an additional basis set cut-off was applied based on the polyad number,

$$P = 2(n_1 + n_2) + n_3 \leq P_{\max} \quad (22)$$

which used the polyad cutoff $P_{\max} = 24$. The maximal values of n_1, n_2 and n_3 that define the size of the primitive basis set were 12, 12 and 24, respectively. The contracted $J = 0$ basis set contained 192 and 143 basis functions with energies up to $16\,000\text{ cm}^{-1}$ for the A_1 and B_2 symmetries, respectively. For the rotational basis set, symmetrized spherical harmonics were used [40].

Line list calculations employed the empirically refined PES (discussed below) and *ab initio* DMS. All transitions and corresponding line strengths were computed for the $0\text{--}10\,000\text{ cm}^{-1}$ range with a lower state energy threshold of $10\,000\text{ cm}^{-1}$ and upper state threshold of $18\,000\text{ cm}^{-1}$. States were computed up to $J = 60$ but only those below $J = 51$ contributed to the line list with the $J > 51$ energies lying above $10\,000\text{ cm}^{-1}$. The nuclear spin statistical weights of $^{28}\text{Si}^1\text{H}_2$ are $g_{(\text{ns})} = \{1, 1, 3, 3\}$ for states of symmetry $\{A_1, A_2, B_1, B_2\}$, respectively. Atomic mass values were used for the TROVE calculations.

2.4. Potential energy surface refinement

To improve the accuracy of the computed line list the initial *ab initio* PES was empirically refined using an efficient least-squares fitting procedure [46] implemented in TROVE. Experimental term values up to $J = 5$ were extracted from the literature [47–50] and these are listed in Table 1. Since spectroscopic data for the ground electronic state is very limited, additional term values of the ν_2 bending mode were generated using the spectroscopic constants from Ref. [47] with the PGOPHER program [51]. Pure rotational energies up to $J = 5$ were generated in a similar manner using the spectroscopic constants of Ref. [47]. We mention that in some instances we have extracted the ‘perturbed’ band origins, i.e. those directly observed in experiment and not the ‘unperturbed’ values fitted in the analysis along with resonance/coupling parameters. For example, in Ref. [49] the perturbed ν_1 fundamental is at 2005.4692 cm^{-1} , while the unperturbed band origin is given as 1995.9280 cm^{-1} .

Table 1: Results of the potential energy surface (PES) refinement. Observed term values are compared against those computed with the *ab initio* and refined PESs. Each energy level is described by seven (standard) quantum numbers and has been assigned a weight in the refinement (see text). The TROVE assignment of the three entries marked with an ^a disagree with the experimental assignment. The term values marked with a ^b, referenced by [49], are from an unpublished work. Term values from Ref. [47] were generated with their spectroscopic constants using the program PGOPHER [51]. The experimental term values from Ref. [50] were shifted by -3.5 cm^{-1} (see text).

Observed	<i>Ab initio</i>	Refined	Δ_{abinit}	Δ_{ref}	Wt.	<i>J</i>	Γ	K_a	K_c	v_1	v_2	v_3	Ref.
998.6241	998.177	998.608	0.447	0.016	1.000	0	A_1	0	0	0	1	0	[47]
1992.816	1996.464	1993.000	-3.648	-0.184	0.100	0	B_2	0	0	0	0	1	[49] ^b
2005.4692	2008.831	2005.357	-3.361	0.112	0.100	0	A_1	0	0	1	0	0	[49]
2952.7	2953.933	2951.678	-1.233	1.022	0.010	0	A_1	0	0	0	3	0	[48] ^a
2998.6	3001.685	2998.785	-3.085	-0.185	0.010	0	A_1	0	0	1	1	0	[48] ^a
3907.4	3914.162	3907.789	-6.762	-0.389	0.010	0	A_1	0	0	1	2	0	[48]
3923.3	3930.305	3923.642	-7.005	-0.342	0.010	0	A_1	0	0	2	0	0	[48]
3976.8	3981.070	3975.988	-4.270	0.812	0.010	0	B_2	0	0	1	0	1	[48] ^a
3997.5	4004.096	3996.334	-6.596	1.166	0.010	0	A_1	0	0	0	0	2	[48]
1010.64	1010.205	1010.627	0.433	0.011	1.000	1	A_2	1	1	0	1	0	[50]
1990.12	1992.097	1990.346	-1.978	-0.228	0.010	1	A_2	1	1	0	2	0	[50]
2017.32	2020.688	2017.434	-3.369	-0.115	0.010	1	A_2	1	1	1	0	0	[50]
2964.02	2966.188	2963.896	-2.169	0.122	0.010	1	A_2	1	1	0	3	0	[50]
3010.78	3013.822	3010.941	-3.043	-0.162	0.010	1	A_2	1	1	1	1	0	[50]
3919.02	3926.280	3919.667	-7.261	-0.648	0.010	1	A_2	1	1	2	0	0	[50]
3935.95	3942.153	3935.672	-6.204	0.277	0.002	1	A_2	1	1	0	0	2	[50]
3987.83	3993.210	3987.986	-5.381	-0.157	0.002	1	A_2	1	1	1	0	0	[50]
4008.23	4015.819	4008.194	-7.590	0.035	0.002	1	A_2	1	1	0	0	1	[50]
4873.99	4880.069	4873.381	-6.080	0.608	0.001	1	A_2	1	1	1	3	0	[50]
4901.48	4908.368	4901.882	-6.889	-0.403	0.001	1	A_2	1	1	2	1	0	[50]
4953.24	4959.496	4953.837	-6.257	-0.598	0.001	1	A_2	1	1	1	1	1	[50]
4989.73	4996.392	4990.789	-6.663	-1.060	0.001	1	A_2	1	1	1	1	1	[50]
5819.86	5826.200	5818.389	-6.341	1.470	0.001	1	A_2	1	1	1	4	0	[50]
5859.73	5867.706	5860.959	-7.977	-1.230	0.001	1	A_2	1	1	2	2	0	[50]
5967.03	5974.871	5969.095	-7.842	-2.067	0.001	1	A_2	1	1	0	4	1	[50]
6756.18	6764.534	6755.532	-8.355	0.647	0.001	1	A_2	1	1	1	5	0	[50]
6808.93	6819.310	6812.410	-10.381	-3.481	0.001	1	A_2	1	1	2	3	0	[50]
6842.27	6854.335	6842.308	-12.066	-0.039	0.000	1	A_2	1	1	1	3	1	[50]
6883.65	6895.644	6883.496	-11.995	0.153	0.000	1	A_2	1	1	2	1	1	[50]
6935.53	6944.916	6940.619	-9.387	-5.090	0.000	1	A_2	1	1	0	5	1	[50]
11.8007	11.809	11.793	-0.008	0.008	5.000	1	A_2	1	1	0	0	0	[47]
1010.6389	1010.205	1010.627	0.433	0.011	1.000	1	A_2	1	1	0	1	0	[47]
10.7248	10.666	10.721	0.059	0.004	5.000	1	B_1	0	1	0	0	0	[47]
1009.4191	1008.914	1009.393	0.505	0.026	1.000	1	B_1	0	1	0	1	0	[47]
15.1206	15.100	15.123	0.020	-0.003	5.000	1	B_2	1	0	0	0	0	[47]
1014.1412	1013.679	1014.134	0.462	0.007	1.000	1	B_2	1	0	0	1	0	[47]
29.7005	29.592	29.677	0.109	0.023	5.000	2	A_1	0	2	0	0	0	[47]
45.5642	45.530	45.569	0.034	-0.005	5.000	2	A_1	2	0	0	0	0	[47]
1028.4507	1027.900	1028.411	0.551	0.040	1.000	2	A_1	0	2	0	1	0	[47]
1045.4185	1044.956	1045.436	0.462	-0.018	1.000	2	A_1	2	0	0	1	0	[47]
39.8798	39.714	39.886	0.166	-0.006	5.000	2	A_2	1	1	0	0	0	[47]
1039.2223	1038.615	1039.202	0.607	0.020	1.000	2	A_2	1	1	0	1	0	[47]
43.1013	43.135	43.093	-0.033	0.008	5.000	2	B_1	2	1	0	0	0	[47]
1042.8724	1042.479	1042.894	0.393	-0.022	1.000	2	B_1	2	1	0	1	0	[47]
29.9299	29.849	29.904	0.081	0.026	5.000	2	B_2	1	2	0	0	0	[47]
1028.7264	1028.206	1028.692	0.520	0.034	1.000	2	B_2	1	2	0	1	0	[47]
75.2653	75.124	75.248	0.142	0.018	5.000	3	A_1	2	2	0	0	0	[47]
1075.2480	1074.682	1075.243	0.566	0.005	1.000	3	A_1	2	2	0	1	0	[47]
55.8620	55.680	55.804	0.182	0.058	5.000	3	A_2	1	3	0	0	0	[47]
90.1214	90.206	90.111	-0.085	0.010	5.000	3	A_2	3	1	0	0	0	[47]
1054.5509	1053.935	1054.484	0.616	0.067	1.000	3	A_2	1	3	0	1	0	[47]
1091.3028	1090.985	1091.377	0.317	-0.074	1.000	3	A_2	3	1	0	1	0	[47]
55.8286	55.641	55.771	0.187	0.058	5.000	3	B_1	0	3	0	0	0	[47]
83.7307	83.426	83.750	0.305	-0.020	5.000	3	B_1	2	1	0	0	0	[47]
1054.5083	1053.885	1054.440	0.623	0.068	1.000	3	B_1	0	3	0	1	0	[47]
1084.0720	1083.337	1084.064	0.735	0.008	1.000	3	B_1	2	1	0	1	0	[47]
74.1789	73.914	74.172	0.265	0.007	5.000	3	B_2	1	2	0	0	0	[47]
91.6751	91.675	91.678	0.000	-0.003	5.000	3	B_2	3	0	0	0	0	[47]
1073.9511	1073.248	1073.922	0.703	0.029	1.000	3	B_2	1	2	0	1	0	[47]
1092.8609	1092.458	1092.926	0.403	-0.065	1.000	3	B_2	3	0	0	1	0	[47]
89.2630	88.958	89.158	0.305	0.105	5.000	4	A_1	0	4	0	0	0	[47]
132.8721	132.366	132.890	0.507	-0.018	5.000	4	A_1	2	2	0	0	0	[47]
153.7492	153.848	153.744	-0.099	0.006	5.000	4	A_1	4	0	0	0	0	[47]
1087.7457	1087.013	1087.634	0.733	0.111	1.000	4	A_1	0	4	0	1	0	[47]

Table 1: (*Continued*)

Observed	<i>Ab initio</i>	Refined	Δ_{abinit}	Δ_{ref}	Wt.	J	Γ	K_a	K_c	v_1	v_2	v_3	Ref.
1133.9208	1132.984	1133.900	0.937	0.021	1.000	4	A_1	2	2	0	1	0	[47]
1156.7943	1156.528	1156.931	0.266	-0.137	1.000	4	A_1	4	0	0	1	0	[47]
115.6727	115.331	115.633	0.342	0.039	5.000	4	A_2	1	3	0	0	0	[47]
142.4629	142.020	142.497	0.443	-0.034	5.000	4	A_2	3	1	0	0	0	[47]
1115.8104	1115.042	1115.768	0.769	0.043	1.000	4	A_2	1	3	0	1	0	[47]
1144.1973	1143.347	1144.215	0.851	-0.018	1.000	4	A_2	3	1	0	1	0	[47]
115.8995	115.597	115.856	0.303	0.043	5.000	4	B_1	2	3	0	0	0	[47]
152.9005	153.073	152.884	-0.173	0.017	5.000	4	B_1	4	1	0	0	0	[47]
1116.0978	1115.375	1116.062	0.722	0.035	1.000	4	B_1	2	3	0	1	0	[47]
1155.9731	1155.777	1156.119	0.196	-0.145	1.000	4	B_1	4	1	0	1	0	[47]
89.2674	88.964	89.162	0.304	0.105	5.000	4	B_2	1	4	0	0	0	[47]
135.8151	135.614	135.806	0.201	0.009	5.000	4	B_2	3	2	0	0	0	[47]
1087.7515	1087.020	1087.640	0.732	0.111	1.000	4	B_2	1	4	0	1	0	[47]
1137.3989	1136.796	1137.437	0.603	-0.038	1.000	4	B_2	3	2	0	1	0	[47]
164.2316	163.770	164.147	0.462	0.084	5.000	5	A_1	2	4	0	0	0	[47]
211.6531	211.413	211.654	0.240	0.000	5.000	5	A_1	4	2	0	0	0	[47]
1164.5892	1163.715	1164.517	0.874	0.073	1.000	5	A_1	2	4	0	1	0	[47]
1215.2686	1214.656	1215.365	0.613	-0.097	1.000	5	A_1	4	2	0	1	0	[47]
130.0721	129.618	129.906	0.454	0.166	5.000	5	A_2	1	5	0	0	0	[47]
190.7850	190.336	190.760	0.449	0.025	5.000	5	A_2	3	3	0	0	0	[47]
231.4354	231.741	231.410	-0.305	0.025	5.000	5	A_2	5	1	0	0	0	[47]
1128.2434	1127.370	1128.075	0.874	0.169	1.000	5	A_2	1	5	0	1	0	[47]
1192.8474	1192.000	1192.853	0.847	-0.006	1.000	5	A_2	3	3	0	1	0	[47]
1236.8763	1236.852	1237.110	0.024	-0.234	1.000	5	A_2	5	1	0	1	0	[47]
130.0715	129.617	129.906	0.454	0.166	5.000	5	B_1	0	5	0	0	0	[47]
189.9302	189.340	189.919	0.590	0.012	5.000	5	B_1	2	3	0	0	0	[47]
216.3755	215.847	216.421	0.529	-0.045	5.000	5	B_1	4	1	0	0	0	[47]
1128.2426	1127.369	1128.074	0.874	0.169	1.000	5	B_1	0	5	0	1	0	[47]
1191.7737	1190.762	1191.752	1.012	0.021	1.000	5	B_1	2	3	0	1	0	[47]
1219.9643	1219.063	1220.030	0.901	-0.066	1.000	5	B_1	4	1	0	1	0	[47]
164.1932	163.723	164.110	0.470	0.083	5.000	5	B_2	1	4	0	0	0	[47]
205.7064	204.907	205.755	0.799	-0.048	5.000	5	B_2	3	2	0	0	0	[47]
231.8532	232.109	231.835	-0.256	0.018	5.000	5	B_2	5	0	0	0	0	[47]
1164.5381	1163.653	1164.464	0.885	0.074	1.000	5	B_2	1	4	0	1	0	[47]
1208.3132	1207.099	1208.305	1.214	0.009	1.000	5	B_2	3	2	0	1	0	[47]
1237.2663	1237.196	1237.494	0.070	-0.228	1.000	5	B_2	5	0	0	1	0	[47]

During the refinement we noticed an inconsistency in the experimental energy levels from Ref. [50]. For example, their term value 1014.14 cm^{-1} ($0,1,0$), $J_{K_a, K_c} = 1_{11}$ can be compared to a more accurate value $1010.6389 \text{ cm}^{-1}$ from Ref. [47]. Here K_a and K_c are the asymmetric top quantum numbers representing the projections of J along the principal axes a and c , respectively. In fact, after a preliminary fitting to the high resolution data from Refs. [47–49] we noticed a systematic shift of around 3.5 cm^{-1} for all term values from Ref. [50], with the only explanation being miscalibrated experimental energies. We therefore corrected all these term values from Ref. [50] by a constant shift of -3.5 cm^{-1} (the values in Table 1 have been shifted). This improved the quality of the refinement immediately.

In the refinement, the ro-vibrational eigenfunctions of the Hamiltonian constructed with the *ab initio* potential V act as a basis set for solving the ‘perturbed’ ro-vibrational Hamiltonian with the refined potential $V' = V + \Delta V$. The latter is represented using the same expansion as in Eq. (4) so the refined parameters $f'_{ijk} = f_{ijk} + \Delta f_{ijk}$, where the corrections Δf_{ijk} are determined in the fitting. The stability of the refinement is controlled by simultaneously fitting to the original *ab initio* dataset [52], ensuring that

the shape of the PES remains reasonable.

Only 7 expansion parameters were varied in the refinement: the linear parameters f_{100} , f_{001} ; the quadratic parameters f_{200} , f_{101} , f_{110} , f_{002} ; and one cubic parameter f_{003} . The quality of the final PES refinement is detailed in Table 1 and illustrated in Fig. 1. The different weights used in the refinement reflect the experimental uncertainty. Also shown in Table 1 are the variationally computed energy levels using the *ab initio* and refined PESs and the corresponding residuals (observed–calculated), all in cm^{-1} . From Fig. 1 we can clearly see that the refined PES calculations have far smaller residuals compared to the *ab initio* results and that the accuracy of the computed term values has improved. The 100 energy levels used in the refinement were reproduced with an unweighted rms error of 0.73 cm^{-1} compared to the rms error of 3.43 cm^{-1} for the *ab initio* PES. The rotational and ν_2 term values from Ref. [47] were reproduced with an rms error of 0.074 cm^{-1} , the vibrational band centers reported in Ref. [48] were reproduced with an rms error of 0.73 cm^{-1} and the corrected ro-vibrational J_{K_a, K_c} term values from Ref. [50] were reproduced with an rms error of 1.45 cm^{-1} .

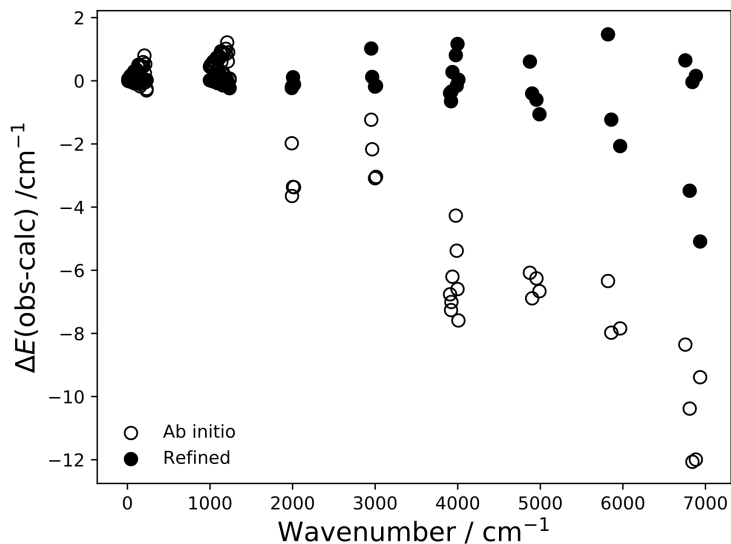


Figure 1: Residuals (observed-calculated) for the *ab initio* (empty circles) and the refined (full circles) term values from Table 1.

The equilibrium geometry was refined to the ground state rotational en-

Table 2: Extract from the `.states` file of the CATS line list

i	\tilde{E}_i	g_i	J	Γ_{tot}	v_1	v_2	v_3	Γ_{vib}	K_a	K_c	τ_{rot}	Γ_{rot}	C_i	n_1	n_2	n_3
1527	19978.952397	3	1	A2	2	8	5	B2	0	1	B1	0.98	2	5	8	
1528	19982.538080	3	1	A2	0	20	1	B2	0	1	B1	0.98	0	1	20	
1529	19986.504561	3	1	A2	10	2	1	B2	0	1	B1	-0.99	0	11	2	
1530	19988.143253	3	1	A2	11	2	0	A1	1	1	A2	0.99	0	11	2	
1531	10.721260	9	1	B1	0	0	0	A1	0	1	B1	1.00	0	0	0	
1532	1009.393331	9	1	B1	0	1	0	A1	0	1	B1	-1.00	0	0	1	
1533	1989.081019	9	1	B1	0	2	0	A1	0	1	B1	1.00	0	0	2	
1534	2004.596674	9	1	B1	0	0	1	B2	1	1	A2	-1.00	0	1	0	
1535	2016.232068	9	1	B1	1	0	0	A1	0	1	B1	1.00	1	0	0	
1536	2962.467155	9	1	B1	0	3	0	A1	0	1	B1	-1.00	0	0	3	

i : State counting number;

\tilde{E}_i : State energy in cm^{-1} ;

g_i : State degeneracy;

J : Total angular momentum quantum number;

Γ_{tot} : Overall symmetry of state in $\mathcal{C}_{2v}(\text{M})$;

v_1 - v_3 : Vibrational (normal mode) quantum numbers;

Γ_{vib} : Vibrational symmetry in $\mathcal{C}_{2v}(\text{M})$;

K_a : Asymmetric top quantum number;

K_c : Asymmetric top quantum number;

τ_{rot} : Rotational parity (0 or 1);

Γ_{rot} : Rotational symmetry in $\mathcal{C}_{2v}(\text{M})$;

C_i : Largest coefficient used in the TROVE assignment;

n_1 - n_3 : Vibrational (TROVE) quantum numbers.

ergy levels up to $J = 5$, yielding the values $r_e = 1.51440 \text{ \AA}$ and $\alpha_e = 92.005^\circ$. These are almost identical to the experimental values $r_{\text{exp}} = 1.5137 \pm 0.0003 \text{ \AA}$ and $\alpha_{\text{exp}} = 92.04 \pm 0.05^\circ$, derived in a combined analysis of high-resolution spectroscopic data of SiH₂, SiHD and SiD₂ [2]. Both the *ab initio* and refined PESs of SiH₂ are provided as part of the supplementary material along with a Fortran routine to construct the surfaces.

3. The CATS line list

The CATS line list contains 254 061 207 transitions connecting 369 973 ro-vibrational states and is provided in the ExoMol data format [17]. Extracts from the `.states` and `.trans` files are given in Tables 2 and 3, respectively. The `.states` file contains all the computed ro-vibrational energy levels (in cm^{-1}). Each level has a unique state counting number, symmetry and quantum number labelling and the contribution C_i from the largest eigen-coefficient used to assign the ro-vibrational state in TROVE. The `.trans` files are split into ten 1000 cm^{-1} wavenumber windows and contain all the computed transitions with upper and lower state ID labels and Einstein A coefficients.

Table 3: Extract from the `.trans` file of the CATS line list

f	i	A_{fi}
149895	153613	1.0606e-06
24599	22431	1.0490e-01
284830	306093	6.3416e-10
74616	84147	6.5034e-08
186408	165765	1.1144e-07
84280	100878	4.1022e-07
224529	228578	2.8423e-04
54609	46478	1.4376e-02
142008	130207	3.6173e-10

f : Upper state ID counting number;
 i : Lower state ID counting number;
 A_{fi} : Einstein A coefficient in s^{-1} .

The normal mode quantum numbers v_1 – v_3 were first reconstructed for $J = 0$ and then propagated to all ro-vibrational states. These are related to the TROVE (local mode) vibrational quantum numbers n_1 – n_3 as follows:

$$v_1 + v_3 = n_1 + n_2 \quad (\text{stretching}), \quad (23)$$

$$v_3 \text{ (odd)} \leftrightarrow (n_1, n_2)B_2, \quad (24)$$

$$v_2 = n_3 \quad (\text{bending}). \quad (25)$$

In correlating the normal mode (v_1, v_3) and local mode (n_1, n_2) pairs we also assumed that the energy increases with v_3 . The asymmetric top quantum number K_a coincides with the TROVE rotational quantum number K . The corresponding quantum number K_c was obtained using the symmetry properties of the oblate rotor [45], see Table 4. Because of the way TROVE builds the symmetrized ro-vibrational basis set [40], the connection between the assignment and the primitive basis functions is not always straightforward and in cases of very small values of $|C_i|$, the assignment should be regarded as indicative.

To illustrate the CATS line list, absorption cross-sections have been generated at 300, 700, 1000, 1500 and 2000 K and the results are shown in Figures 2 and 3. Spectral simulations used a Gaussian line profile and were performed with the ExoCross program [53]. In Fig. 2, the entire computed spectrum of SiH_2 is displayed at logarithmic scale and the linear scale is

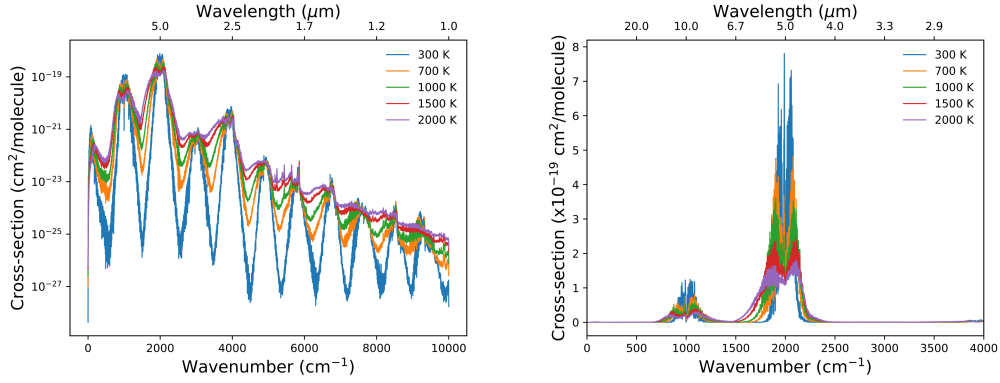


Figure 2: Absorption cross-sections of SiH₂ for various temperatures. Left: 0–10 000 cm⁻¹ range (logarithmic scale); Right: 0–4000 cm⁻¹ range (linear scale). Spectral simulations used a Gaussian line profile with HWHM of 1 cm⁻¹ at a resolution of 1 cm⁻¹.

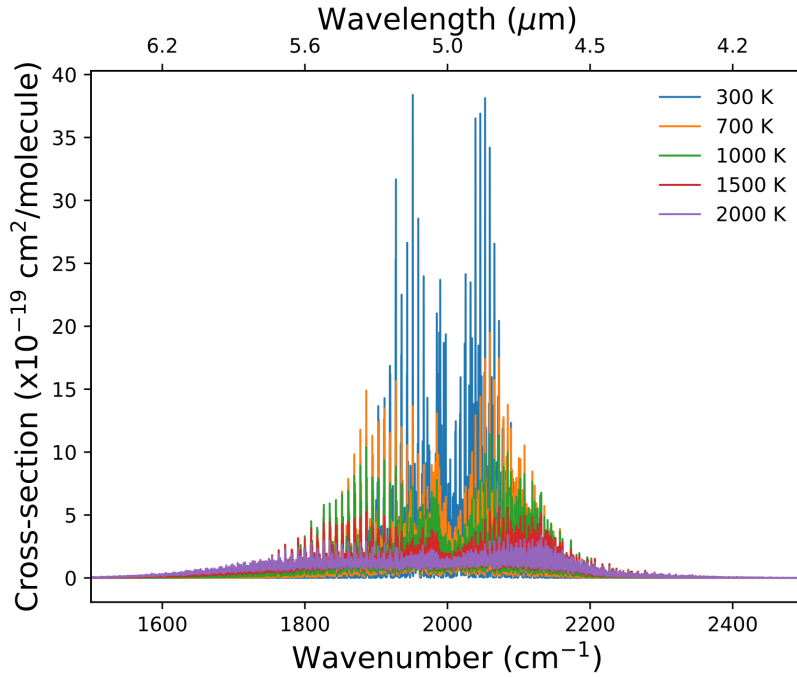


Figure 3: Absorption cross-sections of SiH₂ for various temperatures, focusing on the ν₁ band. Spectral simulations used a Gaussian line profile with HWHM of 0.1 cm⁻¹ at a resolution of 0.1 cm⁻¹.

Table 4: Symmetry properties of the J_{K_a, K_c} states of SiH₂ in the $C_{2v}(M)$ symmetry group [45].

K_a	K_c	Γ_{rot}	K_a	K_c	Γ_{rot}
Even	Even	A_1	Odd	Even	B_2
Even	Odd	B_1	Odd	Odd	A_2

Table 5: Vibrational transition dipole moments (TDM) for the strongest absorption bands of SiH₂ (Debye). The band centers (BC) are theoretical (TROVE) values (cm^{-1}).

Band	BC (cm^{-1})	TDM (Debye)
g.s.	0.00	0.1093
ν_2	998.61	0.1752
$2\nu_2$	1978.35	0.1352
ν_3	1993.00	0.2240
ν_1	2005.54	0.1444
$3\nu_2$	2951.68	0.0029
$\nu_2 + \nu_3$	2974.73	0.0036
$\nu_1 + \nu_2$	2998.78	0.0076
$2\nu_3$	3907.79	0.0102
$\nu_1 + \nu_3$	3913.39	0.0145
$2\nu_1$	3923.64	0.0092
$2\nu_2 + \nu_3$	3952.47	0.0055

displayed up to 4000 cm^{-1} . The strongest bands of SiH₂ are $10 \mu\text{m}$ (ν_2) and $5 \mu\text{m}$ ($2\nu_2$, ν_1 and ν_3), followed by the $2.5 \mu\text{m}$ ($2\nu_1$ and $2\nu_3$) bands, which agrees with the ro-vibrational spectrum from Ref. [12]. The pure rotational band is weak owing to the small equilibrium dipole moment of SiH₂. The corresponding values of the transition dipole moments are listed in Table 5. As the temperature increases, weaker band features become more prominent and the spectrum flattens. This can be seen in closer detail in Fig. 2 and Fig. 3.

The first excited triplet state (\tilde{a}^3B_1) of SiH₂ is around 7000 cm^{-1} [54] while the first excited singlet state (\tilde{A}^1B_1) lies at 15500 cm^{-1} [55]. The presence of these states would have had an effect on the accuracy of the computed *ab initio* PES and DMS, due to Renner-Teller and spin-orbit interactions between these electronic states, which were not taken into account here. Furthermore, the PES was only refined to term values below 7000 cm^{-1} . Use of the CATS line list above 7000 cm^{-1} , or for transitions

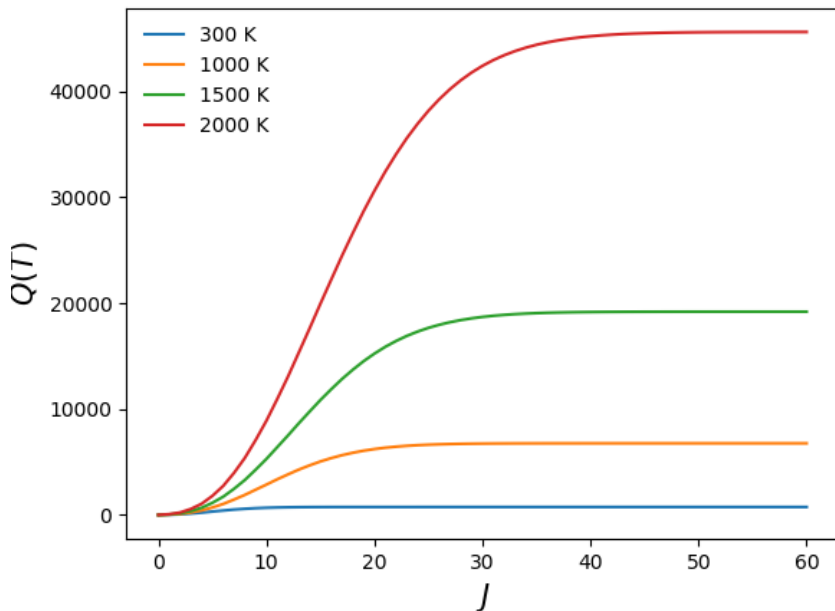


Figure 4: Convergence of the temperature-dependent partition function $Q(T)$ of SiH_2 against the rotational angular momentum quantum number J at 300, 1000, 1500 and 2000 K.

originating from states above 7000 cm^{-1} , should therefore be treated with a degree of caution. That said, the associated transition intensities will be very weak and this should not overly affect the quality of the line list.

3.1. Partition function of silylene

The temperature-dependent partition function,

$$Q(T) = \sum_i g_i \exp\left(-\frac{E_i}{kT}\right), \quad (26)$$

where $g_i = g_i^{(\text{ns})}(2J_i + 1)$ is the degeneracy of a state i with energy E_i and rotational quantum number J_i , has been evaluated at 1 K intervals in the range 0–2000 K. The convergence of $Q(T)$ is illustrated in Fig. 4 for $T = 300, 1000, 1500$ and 2000 K. The flattening of all four lines indicates that convergence has been achieved after approximately $J = 10, 30, 40$ and 50, respectively.

4. Rotational energy level clustering

The equilibrium interbond angle of SiH₂ is close to 90° with the masses of the hydrogen atoms significantly smaller than that of Si. These properties are known to lead to so-called rotational cluster states [56], where a group of rotational energy levels become quasi-degenerate at high rotational excitation. Dorney and Watson [57] were the first to explain cluster formation in terms of classical rotation about symmetrically equivalent axes associated with “stable” axes of rotation, about which the molecule prefers to rotate. Subsequently, Harter and co-workers (see, for example, Refs. [58, 59]) developed classical models for the description of cluster formation in XY_N molecules and introduced the concept of a rotational energy surface (RES), which defines the pattern of the rotational energy levels. The clustering of two or four quasi-degenerate energy levels corresponds classically to the appearance of two or four stable rotation axes, where clockwise and anticlockwise rotations are regarded independently. The two-fold degeneracy is the well known *K*-type doubling [60], while four-fold cluster states in XH₂-type molecules were predicted [23, 61–67] and first observed in the H₂Se molecule [68–70].

In SiH₂, we have found that the rotational energies display typical four-fold clustering behaviour, illustrated in Fig. 5, where we have plotted the reduced rotational energy difference,

$$\tilde{E}_{J,i}^{\text{red}} = \tilde{E}_{J,i} - \tilde{E}_{J,i}^{\text{max}}. \quad (27)$$

Here, $\tilde{E}_{J,i}^{\text{max}}$ is the maximal energy level for a given *J*-manifold, which for SiH₂ corresponds to $K_a = J$. As *J* increases the separation between the two pairs of levels with $K_a = J$ ($K_c = 0$ and $K_c = 1$) and $K_a = J - 1$ ($K_c = 1$ and $K_c = 2$) increases, which is common in asymmetric-top molecules. However, after a critical *J* value of $J_{\text{cr}} \approx 17$, this separation starts decreasing until four-fold cluster states form. For example, at $J = 40$ in the top cluster (shown in the bottom panel of Fig. 5), the separation between the two pairs is only 0.2 cm⁻¹ but at $J = 50$ this gap is reduced to 0.006 cm⁻¹. The pattern of the rotational energy levels in Fig. 5 is typical of most XH₂-type molecules [64, 66, 67, 69, 71].

As mentioned above, the four-fold clusters at high *J* can be associated with the formation of stable rotation axes around the molecular bonds Si–H₁ and Si–H₂ with four equivalent rotational motions: clockwise/anticlockwise around the Si–H₁ and Si–H₂ bonds. These rotation axes are approximately

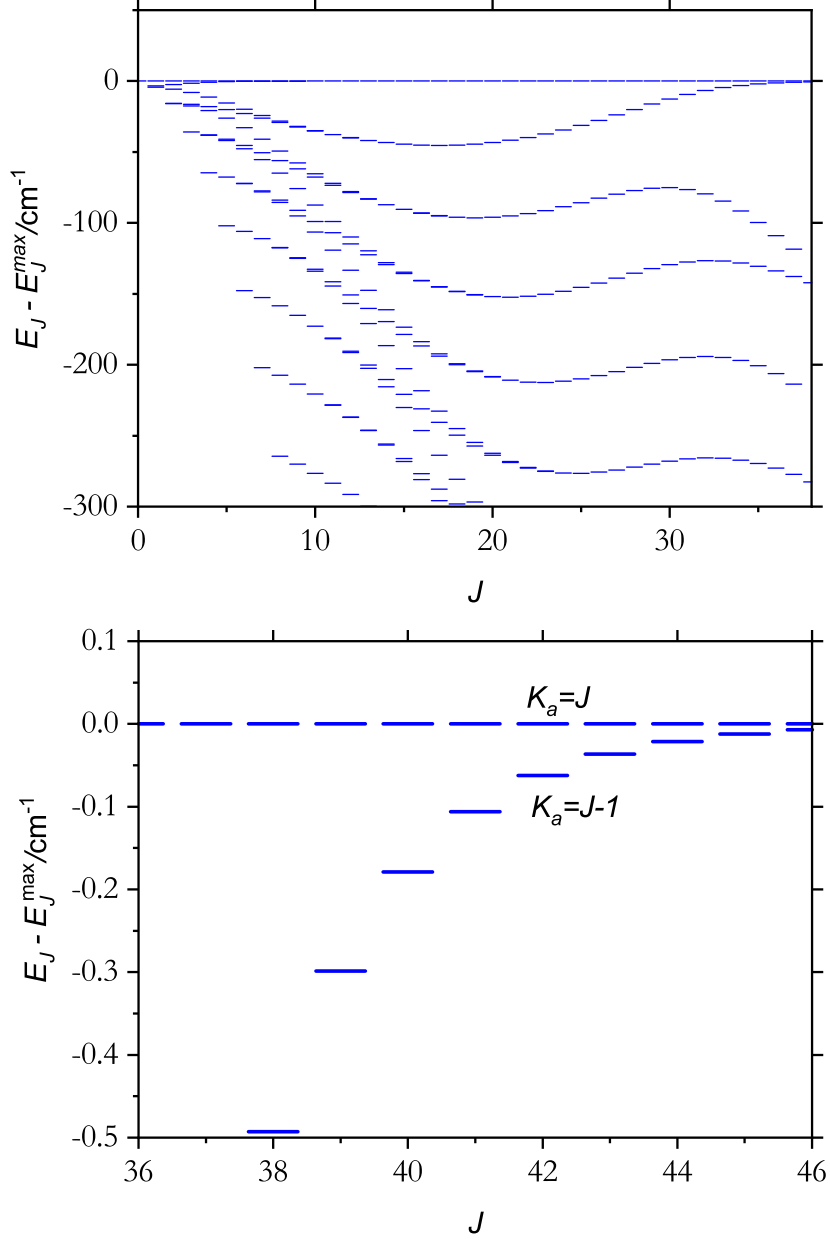


Figure 5: Rotational energy level clustering in the ground vibrational state of SiH_2 . In the top panel, the energy difference $\tilde{E}_{J,i} - \tilde{E}_{J,i}^{\max}$, see Eq. (27), has been plotted for each rotational state, with energy $\tilde{E}_{J,i}$ relative to the maximum energy $\tilde{E}_{J,i}^{\max}$ in its J multiplet. After a certain critical J value the energy difference begins to decrease leading to the formation of four-fold rotational cluster states. A close up of the first cluster state being formed is shown in the bottom panel.

at 45° relative to the principal axes of the molecule x axis (along the bisector) and z axis (in plane). The other stable rotational direction is around the axis associated with the x axis. The rotational motion is commonly illustrated using the rotational energy surface $E_{\theta,\phi}$ [58, 59], constructed as the minimum ro-vibrational energy for each orientation of the angular momentum vector \vec{J} considered in the molecule-fixed axis system, where the orientation is described by a polar angle θ and an azimuthal angle ϕ . Here $\theta \in [0, \pi]$ is the angle between \vec{J} and the molecule-fixed z axis and $\phi \in [0, 2\pi]$ is the angle between the x axis and the projection of \vec{J} in the xy plane, measured in the usual positive sense. In this picture, the RES is a manifestation of the pure rotational motion of a molecule with the vibrational motion completely frozen to the corresponding optimized geometry. If the rotational motion is classically represented by trajectories on the RES, the stationary points (zero-dimensional trajectories) represent rotation about the stabilization axes.

For SiH_2 , we have constructed the RES from a classical ro-vibrational Hamiltonian H_{rv} with the xyz components of the quantum-mechanical angular momentum operator \mathbf{J} substituted by their classical analogues,

$$J_x = \sqrt{J(J+1)} \sin \theta \cos \phi \quad (28)$$

$$J_y = \sqrt{J(J+1)} \sin \theta \sin \phi \quad (29)$$

$$J_z = \sqrt{J(J+1)} \cos \theta, \quad (30)$$

with the generalized momenta $p_n = \partial T / \partial \dot{q}_n$ set to zero [68]. Here, T is the classical kinetic energy and the momentum p_n for $n = 1, 2, 3$ is conjugate to the generalized coordinate $q_n \in \{r_1, r_2, \alpha\}$. The classical Hamiltonian H_{rv} was defined as the same Hamiltonian used in variational TROVE calculations. The RES $E_J(\theta, \phi)$ is then given by [72, 73]

$$E_J(\theta, \phi) = H_{\text{rv}}(J, r_i = r_i^{\text{opt}}, \alpha = \alpha^{\text{opt}}, \theta, \phi), \quad (31)$$

where the classical Hamiltonian function H_{rv} is calculated at the optimized geometries $r_i^{\text{opt}}, \alpha^{\text{opt}}$ for each orientation of the angular momentum defined by the polar and azimuthal angles (θ, ϕ) . The RES was computed on a regular grid of angular points θ_m, ϕ_m . The bond lengths r_1 and r_2 and the bond angle α were optimized at each grid point by minimizing the classical energy $E = H_{\text{rv}}(r_i, \alpha_i, \theta_m, \phi_m)$.

The RES of SiH_2 at $J = 40$ is shown in Figs. 6 and 7, computed on a 40×80 grid (θ, ϕ) of points. The two minima ($\theta = 0$ and 180°) and four

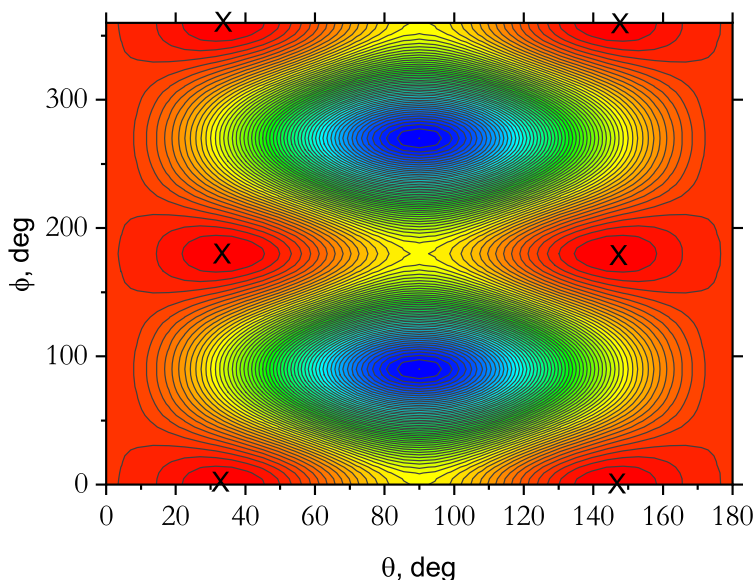


Figure 6: The rotational energy surface of SiH_2 calculated at $J = 40$. The four equivalent maxima corresponding to the four-fold rotational clusters are indicated with crosses. The colour (red to blue) represents the energy scale (high to low).

maxima ($\theta = 36^\circ$ and $\theta = 144^\circ$, $\phi = 0^\circ$ and 180°) form the stationary points of the semi-classical description of the rotation of SiH_2 and can be used to interpret the rotational clustering in the quantum-mechanical description: n -fold degenerate energy clusters [58, 74] correspond to a RES with n symmetrically equivalent stationary points. Coriolis-type effects break the \mathcal{C}_{2v} symmetry of the molecule in the cluster states. For example, the optimized geometry corresponding to the stationary point at $\theta = 36^\circ$, $\phi = 0$ ($J = 40$) was found to be $r_1 = 1.519 \text{ \AA}$, $r_2 = 1.648 \text{ \AA}$ and $\alpha = 87^\circ$. See also Ref. [71] on the bifurcation of stationary points and how it affects the formation of rotational energy clusters.

5. Conclusion

The first, comprehensive high-temperature rotation-vibration line list, named CATS, has been calculated for the electronic ground state of SiH_2 using a refined PES and a high level *ab initio* DMS. The line list covers the wavenumber range 0–10 000 cm^{-1} and is applicable for temperatures up to $T = 2000 \text{ K}$ and represent an improvement for the ro-vibrational spectra

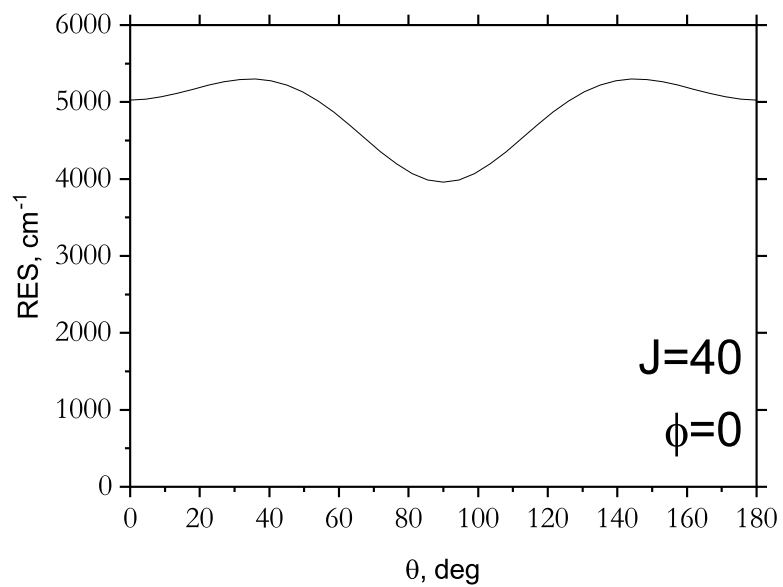


Figure 7: A one-dimensional slice at $\phi = 0^\circ$ of the rotational energy surface (RES) of SiH_2 calculated at $J = 40$ (cm^{-1}). The two equivalent maxima are found at $\theta = 36$ and 144° .

of SiH₂ predicted in Refs. [12, 13]. The CATS line list is available from the ExoMol database [16, 17] at www.exomol.com which already contains line lists for SiH₄ [18] and SiH [19]. There are also recent experimental studies on SiH₃ [6]. These line lists will facilitate spectroscopic studies on silane plasmas. It is also hoped that our work will stimulate more investigations into SiH₂ to enable our theoretical spectroscopic model to be benchmarked and improved upon.

We have demonstrated that SiH₂ forms rotational energy level clusters at high rotational excitation and established the critical J value of $J_{\text{cr}} \approx 17$ when the effect first becomes noticeable. Cluster states are intimately linked to the phenomenon of rotationally-induced chirality in the motion of small polyatomic molecules [75] and the use of techniques from strong-field laser physics [76] can be utilised to produce dynamically chiral molecules through extreme rotational excitation [77].

The CATS line list should find use in plasma physics and the monitoring of SiH₂ in different processes and reactions. Since silylene is a radical and highly reactive, whether it can accumulate in large enough quantities to be detected astronomically is debatable. As discussed above, given the complicated electronic structure of SiH₂ and the relatively low-lying \tilde{a}^3B_1 and \tilde{A}^1B_1 excited states, some caution should be exercised when using the line list above 7000 cm⁻¹, or for transitions originating from states above 7000 cm⁻¹. That said, the associated transition intensities will be very weak and we do not expect the quality of the CATS line list to be significantly affected.

Acknowledgements

This work was supported by UK research councils EPSRC, under grant EP/N509577/1 and STFC, under grant ST/R000476/1. This work made extensive use of UCL's Legion High Performance Computing facility along with the STFC DiRAC HPC facility supported by BIS National E-infrastructure capital grant ST/J005673/1 and STFC grants ST/H008586/1 and ST/K00333X/1.

References

- [1] I. Dubois, G. Herzberg, R. D. Verma, Spectrum of SiH₂, J. Chem. Phys. 47 (10) (1967) 4262. doi:10.1063/1.1701609.
- [2] D. L. Kokkin, T. Ma, T. Steimle, T. J. Sears, Detection and characterization of singly deuterated silylene, SiHD, via optical spectroscopy, J. Chem. Phys. 144 (24) (2016) 244304. doi:10.1063/1.4954702.

- [3] J. Jasinski, B. S. Meyerson, B. A. Scott, Mechanistic studies of chemical vapor-deposition, *Ann. Rev. Phys. Chem.* 38 (1987) 109–140. doi:10.1146/annurev.physchem.38.1.109.
- [4] J. R. Doyle, D. A. Doughty, A. Gallagher, Silane Dissociation Products in Deposition Discharges, *J. Appl. Phys.* 68 (9) (1990) 4375–4384. doi:10.1063/1.346186.
- [5] J. Jasinski, J. O. Chu, Absolute rate constants for the reaction of silylene with hydrogen, silane, and disilane, *J. Chem. Phys.* 88 (1988) 1678–1687. doi:10.1063/1.454146.
- [6] A. S. Nave, A. V. Pipa, P. B. Davies, J. Roepcke, J.-P. H. van Heiden, Determining a Line Strength in the ν_3 Band of the Silyl Radical Using Quantum Cascade Laser Absorption Spectroscopy, *J. Phys. A: Math. Gen.* 123 (46) (2019) 10030–10039. doi:10.1021/acs.jpca.9b06351.
- [7] B. E. Turner, Detection of SiN in IRC + 10216, *Astrophys. J.* 388 (1992) L35. doi:10.1086/186324.
URL <http://adsabs.harvard.edu/doi/10.1086/186324>
- [8] L. W. Avery, M. B. Bell, C. T. Cunningham, P. A. Feldman, R. H. Hayward, J. M. Macleod, H. E. Matthews, J. D. Wade, Submillimeter molecular line observations of IRC+10216: Searches for MgH, SiH₂, and HCO⁺, and detection of hot HCN, *Astrophys. J.* 426 (2,1) (1994) 737–741. doi:10.1086/174110.
- [9] D. D. S. MacKay, S. B. Charnley, The silicon chemistry of IRC+10216, *Mon. Not. R. Astron. Soc.* 302 (4) (1999) 793–800. doi:10.1046/j.1365-8711.1999.02175.x.
URL <https://doi.org/10.1046/j.1365-8711.1999.02175.x>
- [10] Y. Apeloig, R. Pauncz, M. Karni, R. West, W. Steiner, D. Chapman, Why is methylene a ground state triplet while silylene is a ground state singlet?, *Organometallics* 22 (16) (2003) 3250–3256. doi:10.1021/om0302591.
- [11] A. Kalemios, T. H. Dunning, A. Mavridis, SiH₂, a critical study, *Mol. Phys.* 102 (23–24) (2004) 2597–2606. doi:10.1080/00268970412331293802.
- [12] W. Gabriel, P. Rosmus, K. Yamashita, K. Morokuma, P. Palmieri, Theoretical rotational vibrational-spectrum of SiH₂ (X^1A_1 and A^3B_1), *Chem. Phys.* 174 (1) (1993) 45–56. doi:10.1016/0301-0104(93)80050-J.
- [13] S. N. Yurchenko, P. R. Bunker, W. P. Kraemer, P. Jensen, The spectrum of singlet SiH₂, *Can. J. Chem.* 82 (6) (2004) 694–708. doi:10.1139/V04-030.
- [14] R. Guerout, P. R. Bunker, P. Jensen, W. P. Kraemer, A calculation of the rovibronic energies and spectrum of the \tilde{B}^1A_1 electronic state of SiH₂, *J. Chem. Phys.* 123 (24) (2005) 244312. doi:10.1063/1.2139676.
- [15] J. Tennyson, Perspective: Accurate ro-vibrational calculations on small molecules, *J. Chem. Phys.* 145 (2016) 120901. doi:10.1063/1.4962907.
- [16] S. N. Yurchenko, J. Tennyson, ExoMol: molecular line lists for exoplanet and other atmospheres, in: C. Stehlé, C. Jobin, L. d’Hendecourt (Eds.), *European Conference on Laboratory Astrophysics – ECLA*, Vol. 58 of *Euro. Astron. Soc. Publications Series*, 2012, pp. 243–248.
- [17] J. Tennyson, S. N. Yurchenko, A. F. Al-Refaie, E. J. Barton, K. L. Chubb, P. A. Coles, S. Diamantopoulou, M. N. Gorman, C. Hill, A. Z. Lam, L. Lodi, L. K. McKemmish, Y. Na, A. Owens, O. L. Polyansky, T. Rivlin, C. Sousa-Silva, D. S. Underwood, A. Yachmenev, E. Zak, The ExoMol database: molecular line lists for exoplanet and other hot atmospheres, *J. Mol. Spectrosc.* 327 (2016) 73–94. doi:

- 10.1016/j.jms.2016.05.002.
- [18] A. Owens, S. N. Yurchenko, A. Yachmenev, W. Thiel, J. Tennyson, ExoMol molecular line lists XXII. The rotation-vibration spectrum of silane up to 1200 K, *Mon. Not. R. Astron. Soc.* 471 (2017) 5025–5032. doi:10.1093/mnras/stx1952.
 - [19] M. Gorman, S. N. Yurchenko, J. Tennyson, ExoMol Molecular line lists – XXXVI. $X^2\Pi - X^2\Pi$ and $A^2\Sigma^+ - X^2\Pi$ transitions of SH, *Mon. Not. R. Astron. Soc.* 490 (2019) 1652–1665. doi:10.1093/mnras/stz2517/5565070.
 - [20] E. J. Barton, S. N. Yurchenko, J. Tennyson, ExoMol Molecular line lists – II. The ro-vibrational spectrum of SiO, *Mon. Not. R. Astron. Soc.* 434 (2013) 1469–1475.
 - [21] A. Upadhyay, E. K. Conway, J. Tennyson, S. N. Yurchenko, ExoMol Molecular line lists – XXV: A hot line list for silicon sulphide, SiS, *Mon. Not. R. Astron. Soc.* 477 (2018) 1520–1527. doi:10.1093/mnras/sty998.
 - [22] J. Tennyson, S. N. Yurchenko, The ExoMol project: Software for computing molecular line lists, *Intern. J. Quantum Chem.* 117 (2017) 92–103. doi:10.1002/qua.25190.
 - [23] P. Jensen, An introduction to the theory of local mode vibrations, *Mol. Phys.* 98 (17) (2000) 1253–1285. doi:10.1080/002689700413532.
 - [24] C. Hättig, D. P. Tew, A. Köhn, Communications: Accurate and efficient approximations to explicitly correlated coupled-cluster singles and doubles, CCSD-F12, *J. Chem. Phys.* 132 (23) (2010) 231102. doi:10.1063/1.3442368.
 - [25] K. A. Peterson, T. B. Adler, H.-J. Werner, Systematically convergent basis sets for explicitly correlated wavefunctions: The atoms H, He, B–Ne, and Al–Ar, *J. Chem. Phys.* 128 (8) (2008) 084102. doi:10.1063/1.2831537.
 - [26] S. Ten-No, Initiation of explicitly correlated Slater-type geminal theory, *Chem. Phys. Lett.* 398 (1-3) (2004) 56–61. doi:10.1016/j.cplett.2004.09.041.
 - [27] J. G. Hill, K. A. Peterson, G. Knizia, H.-J. Werner, Extrapolating MP2 and CCSD explicitly correlated correlation energies to the complete basis set limit with first and second row correlation consistent basis sets, *J. Chem. Phys.* 131 (19) (2009) 194105. doi:10.1063/1.3265857.
 - [28] K. E. Yousaf, K. A. Peterson, Optimized auxiliary basis sets for explicitly correlated methods, *J. Chem. Phys.* 129 (18) (2008) 184108. doi:10.1063/1.3009271.
 - [29] F. Weigend, A fully direct RI-HF algorithm: Implementation, optimised auxiliary basis sets, demonstration of accuracy and efficiency, *Phys. Chem. Chem. Phys.* 4 (2002) 4285–4291. doi:10.1039/B204199P.
 - [30] C. Hättig, Optimization of auxiliary basis sets for RI-MP2 and RI-CC2 calculations: Core-valence and quintuple-zeta basis sets for H to Ar and QZVPP basis sets for Li to Kr, *Phys. Chem. Chem. Phys.* 7 (2005) 59–66. doi:10.1039/b415208e.
 - [31] H.-J. Werner, P. J. Knowles, G. Knizia, F. R. Manby, M. Schütz, Molpro: a general-purpose quantum chemistry program package, *WIREs Comput. Mol. Sci.* 2 (2012) 242–253. doi:10.1002/wcms.82.
 - [32] V. G. Tyuterev, S. A. Tashkun, D. W. Schwenke, An accurate isotopically invariant potential function of the hydrogen sulphide molecule, *Chem. Phys. Lett.* 348 (2001) 223–234. doi:10.1016/S0009-2614(01)01093-4.
 - [33] H. Partridge, D. W. Schwenke, The determination of an accurate isotope dependent potential energy surface for water from extensive ab initio calculations and experimental data, *J. Chem. Phys.* 106 (1997) 4618–4639. doi:10.1063/1.473987.

- [34] J. K. G. Watson, Robust weighting in least-square fits, *J. Mol. Spectrosc.* 219 (2003) 326–328. doi:10.1016/S0022-2852(03)00100-0.
- [35] P. Jensen, Calculation of rotation-vibration linestrengths for triatomic molecules using a variational approach: Application to the fundamental bands of CH₂, *J. Mol. Spectrosc.* 132 (1988) 429 – 457. doi:http://dx.doi.org/10.1016/0022-2852(88)90338-4.
- [36] U. G. Jørgensen, P. Jensen, The dipole-moment surface and the vibrational transition moments of H₂O, *J. Mol. Spectrosc.* 161 (1993) 219–242. doi:10.1006/jmsp.1993.1228.
- [37] A. A. A. Azzam, L. Lodi, S. N. Yurchenko, J. Tennyson, The dipole moment surface for hydrogen sulfide H₂S, *J. Quant. Spectrosc. Radiat. Transf.* 161 (2015) 41–49. doi:10.1016/j.jqsrt.2015.03.029.
- [38] S. N. Yurchenko, W. Thiel, P. Jensen, Theoretical ROVibrational Energies (TROVE): A robust numerical approach to the calculation of rovibrational energies for polyatomic molecules, *J. Mol. Spectrosc.* 245 (2007) 126–140. doi:10.1016/j.jms.2007.07.009.
- [39] A. Yachmenev, S. N. Yurchenko, Automatic differentiation method for numerical construction of the rotational-vibrational Hamiltonian as a power series in the curvilinear internal coordinates using the Eckart frame, *J. Chem. Phys.* 143 (2015) 014105. doi:10.1063/1.4923039.
- [40] S. N. Yurchenko, A. Yachmenev, R. I. Ovsyannikov, Symmetry adapted ro-vibrational basis functions for variational nuclear motion: TROVE approach, *J. Chem. Theory Comput.* 13 (9) (2017) 4368–4381. arXiv:http://dx.doi.org/10.1021/acs.jctc.7b00506, doi:10.1021/acs.jctc.7b00506. URL http://dx.doi.org/10.1021/acs.jctc.7b00506
- [41] B. V. Noumerov, A method of extrapolation of perturbations, *Mon. Not. R. Astron. Soc.* 84 (1924) 592–602. doi:10.1093/mnras/84.8.592.
- [42] J. W. Cooley, An improved eigenvalue corrector formula for solving the Schrödinger equation for central fields, *Math. Comp.* 15 (1961) 363–374. doi:10.1090/S0025-5718-1961-0129566-X.
- [43] K. L. Chubb, P. Jensen, S. N. Yurchenko, Symmetry adaptation of the rotation-vibration theory for linear molecules, *Symmetry* 10 (5) (2018) 137. doi:10.3390/sym10050137.
- [44] K. L. Chubb, A. Yachmenev, J. Tennyson, S. N. Yurchenko, Treating linear molecule HCCH in calculations of rotation-vibration spectra, *J. Chem. Phys.* 149 (2018) 014101. doi:10.1063/1.5031844.
- [45] P. R. Bunker, P. Jensen, *Molecular Symmetry and Spectroscopy*, 2nd Edition, NRC Research Press, Ottawa, 1998.
- [46] S. N. Yurchenko, R. J. Barber, J. Tennyson, W. Thiel, P. Jensen, Towards efficient refinement of molecular potential energy surfaces: Ammonia as a case study, *J. Mol. Spectrosc.* 268 (2011) 123–129. doi:10.1016/j.jms.2011.04.005.
- [47] C. Yamada, H. Kanamori, E. Hirota, N. Nishiwaki, N. Itabashi, K. Kato, T. Goto, Detection of the silylene ν_2 band by infrared diode laser kinetic spectroscopy, *J. Chem. Phys.* 91 (8) (1989) 4582–4586. doi:10.1063/1.456746.
- [48] H. Ishikawa, O. Kajimoto, Fermi resonance and vibrational analysis of SiH₂ (\tilde{A}^1A_1) based on the LIF excitation-spectra of the $\tilde{A}^1B_1(060) \leftarrow \tilde{A}^1A_1(0\nu''0)$ transitions,

- J. Mol. Spectrosc. 150 (2) (1991) 610–619. doi:10.1016/0022-2852(91)90252-6.
- [49] E. Hirota, H. Ishikawa, The vibrational spectrum and molecular constants of silicon dihydride SiH₂ in the ground electronic state, J. Chem. Phys. 110 (9) (1999) 4254–4257. doi:10.1063/1.478308.
- [50] H. Ishikawa, Y. Muramoto, N. Mikami, Stimulated emission pumping spectroscopy of SiH₂: First observation of the spin-orbit interaction between the \tilde{X}^1A_1 A(1) and the \tilde{a}^3B_1 states, J. Mol. Spectrosc. 216 (1) (2002) 90–97. doi:10.1006/jmsp.2002.8666.
- [51] C. M. Western, PGOPHER: A program for simulating rotational, vibrational and electronic spectra, J. Quant. Spectrosc. Radiat. Transf. 186 (2017) 221–242. doi:10.1016/j.jqsrt.2016.04.010.
- [52] S. N. Yurchenko, M. Carvajal, P. Jensen, F. Herregodts, T. R. Huet, Potential parameters of PH₃ obtained by simultaneous fitting of ab initio data and experimental vibrational band origins, Chem. Phys. 290 (2003) 59–67. doi:10.1016/S0301-0104(03)00098-3.
- [53] S. N. Yurchenko, A. F. Al-Refaie, J. Tennyson, ExoCross: a general program for generating spectra from molecular line lists, Astron. Astrophys. 614 (2018) A131. doi:10.1051/0004-6361/201732531.
- [54] J. Berkowitz, J. P. Greene, H. Cho, B. Rušćić, Photoionization mass spectrometric studies of SiH_n ($n = 1-4$), J. Chem. Phys. 86 (3) (1987) 1235–1248. doi:10.1063/1.452213.
URL <https://doi.org/10.1063/1.452213>
- [55] R. Escribano, A. Campargue, Absorption spectroscopy of SiH₂ near 640 nm, J. Chem. Phys. 108 (15) (1998) 6249–6257. doi:10.1063/1.476062.
- [56] P. Jensen, G. Osmann, I. N. Kozin, The Formation of Four-fold Rovibrational Energy Clusters in H₂S, H₂Se, and H₂Te, in: D. Papoušek (Ed.), Advanced Series in Physical Chemistry: Vibration-Rotational Spectroscopy and Molecular Dynamics, Vol. 9, World Scientific Publishing Company, Singapore, 1997, pp. 298–351.
- [57] A. J. Dorney, J. K. G. Watson, Forbidden Rotational Spectra of Polyatomic-Molecules Stark Effects and $\Delta J = 0$ Transitions of T_d Molecules, J. Mol. Spectrosc. 42 (1972) 135–148. doi:10.1016/0022-2852(72)90150-6.
- [58] W. G. Harter, C. W. Patterson, Rotational Energy Surfaces and High- J Eigenvalue Structure of Polyatomic-Molecules, J. Chem. Phys. 80 (1984) 4241–4261. doi:10.1063/1.447255.
- [59] W. G. Harter, Computer Graphical and Semiclassical Approaches to Molecular Rotations and Vibrations, Comp. Phys. Rep. 8 (1988) 319–394. doi:10.1016/0167-7977(88)90011-1.
- [60] D. Papoušek, M. R. Aliev, Molecular Vibrational-Rotational Spectra, Elsevier, Amsterdam, 1982.
- [61] B. I. Zhilinsky, I. M. Pavlichenkov, Critical Effect in Rotational Spectra of Water Molecule, Opt. Spektrosk. 64 (1988) 688–690.
- [62] K. K. Lehmann, The interaction of rotation and local mode tunneling in the overtone spectra of symmetrical hydrides, J. Chem. Phys. 95 (4) (1991) 2361–2370. doi:10.1063/1.460942.
- [63] I. N. Kozin, S. Klee, P. Jensen, O. L. Polyansky, I. M. Pavlichenkov, The Far-Infrared Fourier-Transform Spectrum of H₂Se, J. Mol. Spectrosc. 158 (1993) 409–

422. doi:10.1006/jmsp.1993.1085.
- [64] I. N. Kozin, P. Jensen, Fourfold Clusters of Rovibrational Energy-Levels for H₂S Studied With a Potential-Energy Surface Derived From Experiment, *J. Mol. Spectrosc.* 163 (1994) 483–509. doi:10.1006/jmsp.1994.1041.
- [65] I. N. Kozin, I. M. Pavlichenkov, Bifurcation in rotational spectra of nonlinear AB₂ molecules, *J. Chem. Phys.* 104 (1996) 4105–4113. doi:10.1063/1.471223.
- [66] I. N. Kozin, P. Jensen, O. Polanz, S. Klee, L. Poteau, J. Demaison, The Rotational Spectrum of H₂Te, *J. Mol. Spectrosc.* 180 (2) (1996) 402–413.
- [67] P. Gómez, L. Pacios, P. Jensen, Fourfold Clusters of Rovibrational Energies in H₂Po Studied with an *Ab Initio* Potential Energy Function, *J. Mol. Spectrosc.* 186 (1) (1997) 99 – 104. doi:https://doi.org/10.1006/jmsp.1997.7434.
URL <http://www.sciencedirect.com/science/article/pii/S0022285297974348>
- [68] I. N. Kozin, P. Jensen, Fourfold Clusters of Rovibrational Energy-Levels in the Fundamental Vibrational-States of H₂Se, *J. Mol. Spectrosc.* 161 (1993) 186–207. doi:10.1006/jmsp.1993.1226.
- [69] P. Jensen, I. N. Kozin, The Potential-Energy Surface for the Electronic Ground-State of H₂Se Derived from Experiment, *J. Mol. Spectrosc.* 160 (1993) 39–57. doi:10.1006/jmsp.1993.1155.
- [70] J. M. Flaud, C. Camy-Peyret, H. Burger, P. Jensen, I. N. Kozin, Experimental-Evidence for the Formation of Fourfold Rovibrational Energy Clusters in the ν_1/ν_3 Vibrational-States of H₂⁸⁰Se, *J. Mol. Spectrosc.* 172 (1995) 126–134. doi:10.1006/jmsp.1995.1161.
- [71] I. M. Pavlichenkov, B. I. Zhilinskií, Critical phenomena in rotational spectra, *Ann. Phys.* 184 (1988) 1–32. doi:10.1016/0003-4916(88)90268-0.
- [72] S. N. Yurchenko, W. Thiel, S. Patchkovskii, P. Jensen, Theoretical evidence for the formation of rotational energy level clusters in the vibrational ground state of PH₃, *Phys. Chem. Chem. Phys.* 7 (2005) 573–582. doi:10.1039/b418073a.
- [73] S. N. Yurchenko, W. Thiel, P. Jensen, Rotational energy cluster formation in XY₃ molecules: Excited vibrational states of BiH₃ and SbH₃, *J. Mol. Spectrosc.* 240 (2006) 174–187. doi:10.1016/j.jms.2006.10.002.
- [74] J. Makarewicz, Semiclassical and quantum mechanical pictures of the ro-vibrational motion of triatomic molecules, *Mol. Phys.* 69 (5) (1990) 903–921. arXiv:https://doi.org/10.1080/00268979000100681, doi:10.1080/00268979000100681.
URL <https://doi.org/10.1080/00268979000100681>
- [75] P. R. Bunker, P. Jensen, Chirality in rotational energy level clusters, *J. Mol. Spectrosc.* 228 (2004) 640–644. doi:10.1016/j.jms.2004.02.027.
- [76] A. Owens, A. Yachmenev, J. Küpper, Coherent control of the rotation axis of molecular superrotors, *J. Phys. Chem. Lett.* 9 (15) (2018) 4206–4209. doi:10.1021/acs.jpcllett.8b01689.
URL <https://doi.org/10.1021/acs.jpcllett.8b01689>
- [77] A. Owens, A. Yachmenev, S. N. Yurchenko, J. Küpper, Climbing the rotational ladder to chirality, *Phys. Rev. Lett.* 121 (2018) 193201. doi:10.1103/PhysRevLett.121.193201.